Article

Cosmological Parameter Estimation Using Current and Future Observations of Strong Gravitational Lensing

Jing-Zhao Qi [1] , Wei-Hong Hu [1], Yu Cui [1], Jing-Fei Zhang [1] and Xin Zhang [1,2,3,*]

1 Department of Physics, College of Sciences, Northeastern University, Shenyang 110819, China; qijingzhao@mail.neu.edu.cn (J.-Z.Q.); huweihong@stumail.neu.edu.cn (W.-H.H.); cuiyuu@stumail.neu.edu.cn (Y.C.); jfzhang@mail.neu.edu.cn (J.-F.Z.)
2 Frontiers Science Center for Industrial Intelligence and Systems Optimization, Northeastern University, Shenyang 110819, China
3 Key Laboratory of Data Analytics and Optimization for Smart Industry, Northeastern University, Ministry of Education, Shenyang 110819, China
* Correspondence: zhangxin@mail.neu.edu.cn

Abstract: The remarkable development of cosmology benefits from the increasingly improved measurements of cosmic distances, including absolute distances and relative distances. In recent years, however, the emerged cosmological tensions have motivated us to explore independent and precise late-universe probes. The two observational effects of strong gravitational lensing (SGL), the velocity dispersions of lens galaxies and the time delays between multiple images can provide measurements of relative and absolute distances, respectively, and their combination makes it possible to break the degeneracies between cosmological parameters and enable tight constraints on them. In this paper, we combine the observed 130 SGL systems with velocity-dispersion measurements and 7 SGL systems with time-delay measurements to constrain dark-energy cosmological models. It is found that the combination of the two effects does not significantly break the degeneracies between cosmological parameters as expected. However, with the simulations of 8000 SGL systems with well-measured velocity dispersions and 55 SGL systems with well-measured time delays based on the forthcoming LSST survey, we find that the combination of two effects can significantly break the parameter degeneracies, and make the constraint precision of cosmological parameters meet the standard of precision cosmology. We conclude that the observations of SGL will become a useful late-universe probe for precisely measuring cosmological parameters.

1. Introduction

The remarkable development of cosmology has benefited from the increasingly improved measurements of cosmic distances as a function of redshift. For instance, precise measurements of anisotropies in cosmic microwave background (CMB) radiation provide tight constraints on the acoustic horizon scale corresponding to the distance that sound waves have travelled till the last scattering, which enables the constraints on several fundamental cosmological parameters to be achieved with breathtaking precision [1–3]. Type Ia supernovae (SNe Ia) as standard candles could provide the relative luminosity distances, and the measurements of them led to the discovery of dark energy [4,5]. In addition, the baryon acoustic oscillation (BAO) as the standard ruler can be used to determine angular diameter distances [6,7]. However, it should be noted that the inherent scale for BAO standard ruler needs to be calibrated by CMB. Therefore, strictly speaking, the measurements of BAO are essentially also the relative distances.

The measurement of absolute distances is difficult but is important because the determination of one of the most fundamental parameters in cosmology, the Hubble constant H_0, is

closely related to it. Moreover, recently, the measurement inconsistencies associated with H_0 are posing a serious challenge to modern cosmological theory [8–22]. The measurements of CMB power spectra by the Planck satellite infer the value of $H_0 = 67.4 \pm 0.5$ km s^{-1} Mpc^{-1} assuming a flat Λ cold dark matter (ΛCDM) model. However, in the local universe, the measured absolute distances of SNe Ia calibrated by distance ladders yield a larger value of $H_0 = 74.03 \pm 1.42$ km s^{-1} Mpc^{-1} [23]. Above 4σ tension between the values from two independent methods, these cannot be attributed to systematic errors crudely [23,24]. In this context, the Hubble tension further highlights the importance of independent and precise measurements on absolute distances.

Strong gravitational lensing (SGL) can be used to measure an alternative absolute distance, the so-called time-delay distance $D_{\Delta t}$, which is a combination of three angular diameter distances between observer, lens and source. Moreover, with the stellar velocity-dispersion measurements of the lens galaxy, the angular diameter distance D_l from observer to lens can also be obtained. In this way, the H0LiCOW (H_0 Lenses in COSMOGRAIL's Wellspring) team presented a measured value of $H_0 = 73.3^{+1.7}_{-1.8}$ km s^{-1} Mpc^{-1} with a 2.4% precision from the observations of time delay for six lensed quasars [25]. However, due to many difficulties in measuring the time delays of lensed quasars, there are only 7 observed samples at present [26–29]. Even for the future surveys, such as the Large Synoptic Survey Telescope (LSST) with wide field-of-view and frequent time sampling to monitor the SGL systems for time-delay measurements [30,31], are predicted to observe only a few dozen samples of well-measured SGL time delay [32–34]. The small sample size makes it difficult to use as a powerful statistical quantity to precisely constrain cosmology.

In fact, for the galaxy-scale SGL samples, in addition to the time-delay measurements, several observed quantities can be used as the statistical quantities to constrain cosmological parameters, including the distribution of image angular separations [35,36], the distribution of lens redshifts [37–39], and the velocity dispersion of lens galaxies [40–43]. Recently, using the lens velocity dispersion as statistical quantity in cosmology yields a series of achievements [44–54]. With spectroscopic and astrometric data, 161 available samples are obtained with well-defined selection criteria at present [52]. Moreover, according to the predictions of the LSST survey [55–58], more than 1×10^5 lensed galaxies and more than 8×10^3 lensed quasars could potentially be observed. Such a large sample is bound to yield extensive cosmological applications. For this method, the core idea is that the gravitational mass M^E_{grl} equals to the dynamical mass M^E_{dyn} within the Einstein radius θ_E [52]. The inferences of both masses are related to the cosmological distances, and the final formula derived from the equality of the two masses is a function of the distance ratio, D_{ls}/D_s, where D_{ls} is the angular diameter distance between lens and source, and D_s is the one between observer and source. In other words, the measurement provided by this method is relative distance.

In previous studies [43,59–64], the respective applications of the two observed effects of SGL described above in cosmological parameter constraints have been fully discussed, as well as the improvements for parameter constraints by combining with CMB data [32,34,65]. Nevertheless, two incentives encourage us to improve and develop it further. Firstly, instead of the dependence on CMB as the precise early-universe probe to precisely constrain cosmology, to develop independent and precise late-universe probes is of great significance in the context of cosmological tensions indicating the inconsistencies between the early and late universe [66]. Secondly, the determination of H_0 depends on the measurement of absolute distance, while the measurement of relative distance is helpful for constraints on other cosmological parameters such as the present matter density Ω_m and the equation of state of dark energy w [43,59–61]. The combination of two independent observed effects of SGL providing the measurements of absolute distances and relative distances, respectively, is expected to break the cosmological parameter degeneracies and place tight constraints on them. In this paper, we will investigate what improvement the combination of these two observations will have on the cosmological constraint precision and whether a large sample of well-measured SGL data in the future LSST era can be used as a precise late-universe

probe. Here, we consider three typical dark energy models for this analysis, i.e., the ΛCDM model, the wCDM model, and the Chevalliear–Polarski–Linder (CPL) model [67].

2. Methodology and Data

2.1. Velocity Dispersion of Lens Galaxies

The key point of using the lens velocity dispersion (VD) as statistical quantity to constrain cosmological parameters is that the inferred gravitational mass $M_{\mathrm{grl}}^{\mathrm{E}}$ within the Einstein radius is equal to the projected dynamical mass $M_{\mathrm{dyn}}^{\mathrm{E}}$, namely $M_{\mathrm{grl}}^{\mathrm{E}} = M_{\mathrm{dyn}}^{\mathrm{E}}$. With the observations of angular separations between multiple images, the gravitational mass within the Einstein radius θ_{E} could be inferred by

$$M_{\mathrm{grl}}^{\mathrm{E}} = \frac{c^2}{4G} \frac{D_{\mathrm{s}} D_{\mathrm{l}}}{D_{\mathrm{ls}}} \theta_{\mathrm{E}}^2, \tag{1}$$

where D_{s} is the angular diameter distance between observer and source, D_{l} is that between observer and lens, and D_{ls} is that between lens and source.

On the other hand, assuming a mass distribution model for the lens galaxy, the projected dynamical mass $M_{\mathrm{dyn}}^{\mathrm{E}}$ can be derived. The mass distribution of the lens galaxy is closely related to the constraints on cosmological parameters. The actual mass distribution of the lens galaxy is not necessarily an axisymmetric distribution, but a more ellipsoidal non-axisymmetric distribution. The isothermal elliptical model proposed by Kormann et al. [68] is one of the common gravitational lensing models, which has caustics and critical curves in analytical form. Furthermore, ellipsoid models allow an estimation of effects due to the galaxy shape, and it fits well with mass profiles implied by observations [69]. However, elliptical matter distributions are in general more difficult to handle, and here we take a simpler assumption of spherical symmetry. In this paper, we choose a general mass model for the lens galaxies [52,70]:

$$\begin{cases} \rho(r) = \rho_0 \, (r/r_0)^{-\gamma}, \\ \nu(r) = \nu_0 \, (r/r_0)^{-\delta}, \\ \beta_{\mathrm{ani}}(r) = 1 - \sigma_\theta^2/\sigma_r^2, \end{cases} \tag{2}$$

where $\rho(r)$ is the total mass density distribution, and $\nu(r)$ represents the luminous mass density distribution. The parameter $\beta_{\mathrm{ani}}(r)$ characterizes the anisotropy of the stellar velocity dispersion, while σ_θ and σ_r are the tangential and radial velocity dispersions, respectively. For the total mass density slope γ, according to the analysis in Ref. [52], the dependencies of γ on both the redshift and the surface mass density should be taken into account. In this paper, therefore, we also adopt the parameterization of γ as [52]

$$\gamma = \gamma_0 + \gamma_z z_{\mathrm{l}} + \gamma_s \log \tilde{\Sigma}, \tag{3}$$

where γ_0, γ_z and γ_s are constants, and z_{l} is the redshift of lens. Here, $\tilde{\Sigma}$ is the normalized surface mass density, defined as

$$\tilde{\Sigma} = \frac{(\sigma_0/100 \, \mathrm{km \, s^{-1}})^2}{R_{\mathrm{eff}}/10 \, h^{-1} \mathrm{kpc}}, \tag{4}$$

where $h = H_0/(100 \, \mathrm{km \, s^{-1} \, Mpc^{-1}})$, R_{eff} is the half-light radius of the lens galaxy, and σ_0 is the velocity dispersion of the lens galaxy.

For the luminous mass density slope δ, it is commonly considered as a universal parameter for all lens galaxies in the entire sample. In fact, however, the individual value of δ for lens galaxies can be obtained by fitting the two-dimensional power-law luminosity profile over a circle of radius $\theta_{\mathrm{eff}}/2$ for lens galaxies with the high-resolution imaging data. In this way, a sample including 130 SGL systems with the δ observation is obtained [52].

Moreover, Chen et al. [52] concluded that the intrinsic scatter of δ among the lenses should be taken into account to obtain an unbiased cosmological estimate.

By combining the mass distribution model in Equation (2) and the well-known spherical Jeans equation, the total mass contained within a sphere with radius r can be expressed as

$$
M(r) = \frac{2}{\sqrt{\pi}} \frac{\Gamma(\gamma/2)}{\Gamma(\frac{\gamma-1}{2})} \left(\frac{r}{R_{\mathrm{E}}}\right)^{3-\gamma} M_{\mathrm{dyn}}^{\mathrm{E}},
\tag{5}
$$

where the Einstein radius R_{E} is determined by $R_{\mathrm{E}} = D_{\mathrm{l}}\theta_{\mathrm{E}}$ [42], and $\Gamma(x)$ is Euler's Gamma function. The radial velocity dispersion σ_r is determined by

$$
\sigma_r^2(r) = \frac{2}{\sqrt{\pi}} \frac{G M_{\mathrm{dyn}}^{\mathrm{E}}}{R_{\mathrm{E}}} \frac{1}{\xi - 2\beta_{\mathrm{ani}}} \frac{\Gamma(\gamma/2)}{\Gamma(\frac{\gamma-1}{2})} \left(\frac{r}{R_{\mathrm{E}}}\right)^{2-\gamma},
\tag{6}
$$

where $\xi = \gamma + \delta - 2$, and β_{ani} is assumed to be independent of the radius r.

From the spectroscopic data, the velocity dispersion σ_{ap} inside the circular aperture with the angular radius θ_{ap} could be measured. However, to consider the effect of the aperture size on the measurements of velocity dispersions, the velocity dispersion σ_{ap} measured within certain apertures θ_{ap} should be normalized to a typical physical aperture via

$$
\sigma_0 = \sigma_{\mathrm{ap}} [\theta_{\mathrm{eff}}/(2\theta_{\mathrm{ap}})]^{\eta}.
\tag{7}
$$

According to Refs. [52,70,71], the value of correction factor η we adopt is $\eta = -0.066 \pm 0.035$. Based on the above analysis, the velocity dispersion could be expressed as

$$
\sigma_0 = \sqrt{\frac{c^2}{2\sqrt{\pi}} \frac{D_{\mathrm{s}}}{D_{\mathrm{ls}}} \theta_{\mathrm{E}} F(\gamma, \delta, \beta_{\mathrm{ani}}) \left(\frac{\theta_{\mathrm{eff}}}{2\theta_{\mathrm{E}}}\right)^{2-\gamma}},
\tag{8}
$$

where

$$
\begin{aligned}
F(\gamma, \delta, \beta_{\mathrm{ani}}) = {} & \frac{3-\delta}{(\xi - 2\beta_{\mathrm{ani}})(3-\xi)} \\
& \times \left[\frac{\Gamma[(\xi-1)/2]}{\Gamma(\xi/2)} - \beta_{\mathrm{ani}} \frac{\Gamma[(\xi+1)/2]}{\Gamma[(\xi+2)/2]}\right] \\
& \times \frac{\Gamma(\gamma/2)\Gamma(\delta/2)}{\Gamma[(\gamma-1)/2]\Gamma[(\delta-1)/2]}.
\end{aligned}
\tag{9}
$$

For the detailed derivation and description, we refer the reader to Refs. [52,70].

Considering the extra mass contribution from matters along the line of sight (LOS), we take about 3% fractional uncertainty on velocity dispersion as the systematic error $\Delta\sigma_0^{\mathrm{sys}}$ [72]. Together with the statistical error propagated from the measurement error $\Delta\sigma_0^{\mathrm{stat}}$ and the error caused by the aperture correction $\Delta\sigma_0^{\mathrm{AC}}$, the total uncertainty of σ_0 could be given by

$$
(\Delta\sigma_0^{\mathrm{tot}})^2 = (\Delta\sigma_0^{\mathrm{stat}})^2 + (\Delta\sigma_0^{\mathrm{AC}})^2 + (\Delta\sigma_0^{\mathrm{sys}})^2.
\tag{10}
$$

The cosmological parameters could be constrained by maximizing the likelihood $\mathcal{L}_{\mathrm{VD}} \propto \exp(-\chi_{\mathrm{VD}}^2/2)$, and here χ_{VD}^2 is constructed as

$$
\chi_{\mathrm{VD}}^2 = \sum_{i=1}^{N} \left(\frac{\sigma_{0,i}^{\mathrm{th}} - \sigma_{0,i}^{\mathrm{obs}}}{\Delta\sigma_{0,i}^{\mathrm{tot}}}\right)^2,
\tag{11}
$$

where N is the number of the data points.

The observational sample of the velocity dispersion used in this paper originally includes 161 galaxy-scale SGL systems compiled by Chen et al. [52]. However, as mentioned above, the intrinsic scatter of δ among the lens galaxies should be taken into account to

obtain an unbiased cosmological estimate. Therefore, the SGL sample we adopt is the truncated sample including 130 SGL systems with the observations of δ. The relevant information necessary to perform statistical analyses for estimating cosmological parameters includes redshifts of lenses (z_l) and sources (z_s), Einstein angle (θ_E), effective radius (θ_{eff}), aperture angular radius (θ_{ap}), measured velocity dispersion (σ_{ap}), and measured luminous mass density slope (δ). The more detailed analyses and descriptions, we refer the reader to Ref. [52]. For convenience, we use the abbreviation "VD" to represent this SGL sample.

2.2. Time-Delay Measurements

For an SGL system, the emitted light rays from the background object (the source) corresponding to the different image positions pass different paths and gravitational potentials, which makes the time delays between the arrival times of the light rays. If the source is variable, time delays between multiple images can be measured by long-term dedicated photometric monitoring [73–77]. The time delay between two images is related to both the time-delay distance and the gravitational potential of the lens galaxy via the relation:

$$\Delta t_{ij} = \frac{D_{\Delta t}}{c} \left[\frac{(\theta_i - \beta)^2}{2} - \psi(\theta_i) - \frac{(\theta_j - \beta)^2}{2} + \psi(\theta_j) \right], \tag{12}$$

where θ_i and θ_j are the coordinates of the images i and j in the lens plane, respectively. The source position, β, and lens potentials, $\psi(\theta_i)$ and $\psi(\theta_j)$, can be determined from the mass model of the system. With the measurements of the time delay Δt, the time-delay distance $D_{\Delta t}$ can be inferred, which is the combination of three angular diameter distances [78–80]:

$$D_{\Delta t} \equiv (1 + z_l) \frac{D_l D_s}{D_{ls}}. \tag{13}$$

It is important to note that the angular diameter distance D_l also could be obtained by combining the time-delay measurements with the stellar velocity dispersion measurements of the lens galaxy, which not only could improve the constraints on the cosmological parameters, but also is helpful to break the mass-sheet degeneracy [34].

In Table 1, we summarize the existing seven SGL systems with measured time delays $D_{\Delta t}$ and the angular diameter distances D_l. The relevant information necessary to perform statistical estimation of cosmological parameters includes the redshifts of lens and source, the posterior distribution of $D_{\Delta t}$ and D_l in the form of Monte Carlo Markov chains (MCMCs). Here, it should be noted that a kernel density estimator is used to compute the posterior distribution $\mathcal{L}_{D_{\Delta t}}$ from MCMCs. The sampling software could be found in the website (https://doi.org/10.5281/zenodo.3633035, accessed on 18 March 2022) and the posterior distributions of $D_{\Delta t}$ and D_l in the form of MCMCs are available in the H0LiCOW website (http://www.h0licow.org, accessed on 18 March 2022). For convenience, we use the abbreviation "TD" to represent the time-delay measurements.

Table 1. $D_{\Delta t}$ and D_l for the seven lenses.

Lens Name	z_l	z_s	$D_{\Delta t}$ (Mpc)	D_l (Mpc)	References
B1608+656	0.6304	1.394	5156^{+296}_{-236}	1228^{+177}_{-151}	[79,81]
RXJ1131−1231	0.295	0.654	2096^{+98}_{-83}	804^{+141}_{-112}	[28,65]
HE 0435−1223	0.4546	1.693	2707^{+183}_{-168}	-	[28,82]
SDSS 1206+4332	0.745	1.789	5769^{+589}_{-471}	1805^{+555}_{-398}	[83]
WFI2033−4723	0.6575	1.662	4784^{+399}_{-248}	-	[27]
PG 1115+080	0.311	1.722	1470^{+130}_{-127}	697^{+186}_{-144}	[28]
DES J0408−5354	0.597	2.375	3382^{+146}_{-115}	1711^{+376}_{-280}	[29,84]

For the angular diameter distances involved in VD and TD measurements, in the framework of a flat universe, their theoretical expresses D_l, D_s and D_{ls} are given by

$$D_l(z_l; \mathbf{p}) = \frac{c}{H_0(1+z_l)} \int_0^{z_l} \frac{dz}{E(z; \mathbf{p})}, \tag{14}$$

$$D_s(z_s; \mathbf{p}) = \frac{c}{H_0(1+z_s)} \int_0^{z_s} \frac{dz}{E(z; \mathbf{p})}, \tag{15}$$

$$D_{ls}(z_l, z_s; \mathbf{p}) = \frac{c}{H_0(1+z_s)} \int_{z_l}^{z_s} \frac{dz}{E(z; \mathbf{p})}, \tag{16}$$

respectively. Here $E(z) \equiv H(z)/H_0$ is the dimensionless Hubble parameter, and $\mathbf{p}$ denotes the parameters of the considered cosmological model.

3. Results and Discussions

The observations of velocity dispersion for SGL systems provide the measurements of relative distances, while the time-delay observations could offer the absolute distances. In this section, we will present the constraints on cosmological models from these two observations derived from SGL systems to see whether they can break the degeneracy between cosmological parameters. Here, we use the `emcee` [85] Python module based on the MCMC analysis to implement the cosmological constraints.

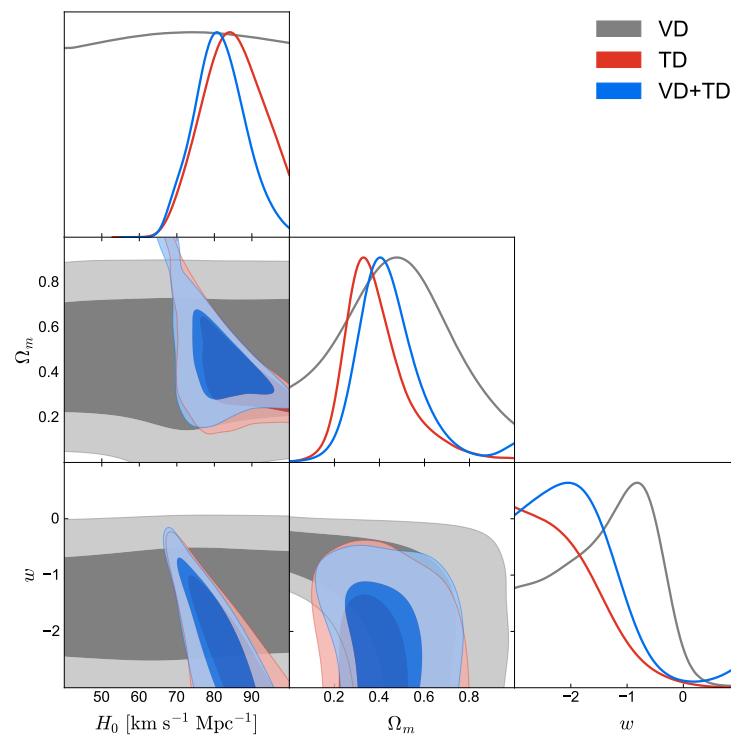### 3.1. The Constraints on Cosmological Parameters with Current Observations of SGL

In Figure 1 and Table 2, we show the constraints on the ΛCDM model from VD, TD and the combination of them, i.e., VD+TD. We can see clearly that the constraint on H_0 from the VD observation is invalid due to the relative distance measurements. The constraint on Ω_m from VD is rather weak, $\Omega_m = 0.400^{+0.256}_{-0.216}$. For the results from the TD observation, the constraint on Ω_m we get is $\Omega_m = 0.362^{+0.247}_{-0.170}$, which is comparable with that from VD. Since TD could measure absolute distances, a tight constraint on H_0 is obtained, i.e., $H_0 = 72.99^{+1.72}_{-2.20}$ km s^{-1} Mpc^{-1}. On the other hand, we can see that the combination of VD and TD does not significantly break the degeneracy between cosmological parameters as expected. The constraint results from VD+TD are $\Omega_m = 0.350^{+0.175}_{-0.139}$ and $H_0 = 73.20^{+1.60}_{-1.86}$ km s^{-1} Mpc^{-1}, from which we can see that the constraints are only slightly improved by the combination.

We present the constraints on the wCDM model in Figure 2 and Table 2. We find that the constraints on Ω_m from VD, TD and VD+TD are similar to those in the case of ΛCDM, for both best-fit values and constraint errors. For H_0, the TD data give $H_0 = 85.29^{+9.75}_{-8.37}$ km s^{-1} Mpc^{-1}. The combination VD+TD gives $H_0 = 81.27^{+7.23}_{-6.64}$ km s^{-1} Mpc^{-1}, and we can see that the data combination only provide a slight improvement because VD cannot effectively constrain H_0. From the posterior probability distribution of w in Figure 2, we can see that the VD data could offer a tighter constraint than TD for the parameter w. The combination VD+TD gives $w = -2.33^{+0.96}_{-1.05}$. We find that a phantom-type dark energy (with $w < -1$) is preferred by the VD+TD data, which leads to a high value of the Hubble constant. Here we also notice that the VD+TD constraint on w is rather weak and its best-fit value significantly deviates from the result $w = -1.03 \pm 0.03$ derived from CMB+BAO+SNe [3]. This is mainly because the current sample sizes of VD and TD are rather small (7 TD data and 130 VD data). Such small-size SGL samples cannot accurately and precisely constrain the EoS of dark energy, and so the current result is much worse than that of CMB+BAO+SNe. On the other hand, the constraints on cosmological parameters depend on accurate modeling of lens models. The mass model of the lens galaxies we adopt is assumed to have a spherical symmetry. The deviation from reality may lead to a bias in estimates of cosmological parameters. Therefore, constructing a more reasonable lens model using future large samples and more accurate observational data is very important for cosmological parameter estimation.

For the CPL model, the constraint results from VD, TD, and VD+TD are shown in Figure 3 and Table 2. Compared with the case of wCDM, the best-fit values and constraint errors of Ω_m, H_0, and w_0 are not changed a lot, even though one more free parameter is added. For w_a, we find that both VD and TD cannot give an effective constraint.
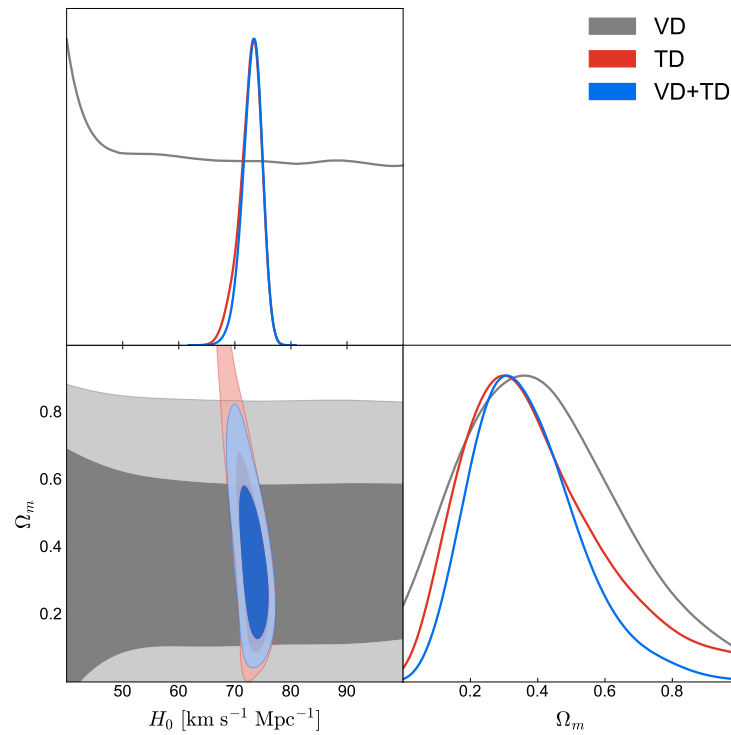
Figure 1. The constraints (68.3% and 95.4% confidence level) on the ΛCDM model from VD, TD, and VD+TD.

Figure 2. The constraints (68.3% and 95.4% confidence level) on the wCDM model from VD, TD, and VD+TD.
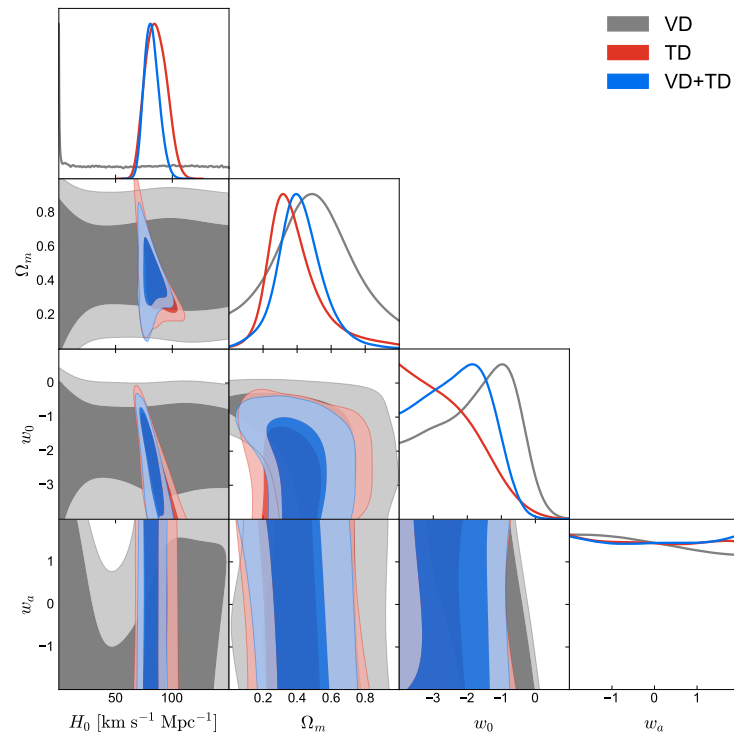
Figure 3. The constraints (68.3% and 95.4% confidence level) on the CPL model from VD, TD, and VD+TD.

Table 2. The constraints on cosmological parameters of the ΛCDM, wCDM and CPL models from the current VD, TD, and VD+TD. Here H_0 is in units of km s^{-1} Mpc^{-1}.

| Model	Parameter	VD	TD	VD+TD
ΛCDM	H_0	-	$72.99^{+1.72}_{-2.20}$	$73.20^{+1.60}_{-1.86}$
	Ω_{m}	$0.400^{+0.256}_{-0.216}$	$0.362^{+0.247}_{-0.170}$	$0.350^{+0.175}_{-0.139}$
wCDM	H_0	-	$85.29^{+9.75}_{-8.37}$	$81.27^{+7.23}_{-6.64}$
	Ω_{m}	$0.471^{+0.250}_{-0.253}$	$0.365^{+0.159}_{-0.102}$	$0.428^{+0.149}_{-0.112}$
	w	$-1.28^{+0.75}_{-1.07}$	$-2.72^{+1.05}_{-0.89}$	$-2.33^{+0.96}_{-1.05}$
CPL	H_0	-	$85.30^{+9.95}_{-9.26}$	$81.46^{+7.00}_{-6.17}$
	Ω_{m}	$0.490^{+0.232}_{-0.235}$	$0.359^{+0.175}_{-0.110}$	$0.410^{+0.137}_{-0.116}$
	w_0	$-1.67^{+1.04}_{-1.46}$	$-2.68^{+1.16}_{-0.93}$	$-2.28^{+0.96}_{-1.11}$
	w_a	$-0.091^{+1.403}_{-1.296}$	$-0.025^{+1.387}_{-1.359}$	$0.010^{+1.367}_{-1.379}$

3.2. Forecast for the Constraints on Cosmological Parameters with the Future Observations

In this subsection, we make a forecast for the constraints on cosmological parameters with the future SGL observations.

According to some estimates, the LSST will observe more than 8000 lensed quasars, about 3000 of which have well-measured time delays during the 10-year survey duration [55–58]. Such a large sample is bound to bring a significant improvement for the estimation of cosmological parameters. Therefore, we perform a simulation for a realistic population of SGL. For the estimate of velocity dispersion, we simulate 8000 well-measured SGL systems with the 5% and 1% uncertainties for the observed velocity dispersion and Einstein radius, respectively, according to the analysis from Ref. [47]. On the other hand, for the measurement of time delay, the sample requires accurate characterization for the mass distribution of the lens galaxy, auxiliary data such as high-resolution imaging, and stellar velocity dispersion observations. By selecting with strict criteria [32,33], there will be about 55 SGL systems with well-measured time-delay distance $D_{\Delta t}$ and angular diameter distances D_l. According to the constraints on current lensed quasars [27–29,65,86], we set 5% uncertainties for the time-delay measurements, 3% for the lens mass modelling uncertainties, and 3% for the lens environment uncertainties, all of which assign 6.6% uncertainty to the time-delay distances for each SGL system [87]. For the precision on D_l, we set 5% uncertainty for it as in Refs. [32,33,87]. In this simulation, we adopt the ΛCDM model as a fiducial model with the values of cosmological parameters $\Omega_m = 0.315$ and $H_0 = 67.4 \, \mathrm{km \, s^{-1} \, Mpc^{-1}}$ taken from Planck 2018 results [3].

The one-dimensional marginalized posterior distributions and the two-dimensional contours of parameters from VD, TD, and VD+TD are shown in Figures 4–6. The constraint results of the parameters are listed in Table 3. It can be seen that all best-fit values of parameters are consistent with the fiducial values at 1 σ confidence level as expected. The key issue we wish to investigate is the constraint capability of the TD and VD observations in the future, which could be directly indicated by the constraint errors (1σ) of parameters. We can see clearly that the combination VD+TD could effectively break the degeneracy between H_0 and Ω_m in these three models. In the ΛCDM model, the joint constraint gives the results $\sigma(H_0) = 0.47 \, \mathrm{km \, s^{-1} \, Mpc^{-1}}$ and $\sigma(\Omega_m) = 0.004$, and we find that the precisions have exceeded the Planck 2018 results, meeting the standard of precision cosmology. In the wCDM model, the constraint on w from VD+TD is $\sigma(w) = 0.05$, which is comparable with the result of Planck 2018 TT,TE,EE+lowE+lensing+SNe+BAO, $\sigma(w) = 0.034$ [88]. In fact, from the posterior distribution of w in Figure 5, we find that the TD observation only give a very weak constraint on w, and the tight constraint is mainly contributed by the VD observation. In the CPL model, the TD observation does not provide an effective constraint on w_a, and even the combination VD+TD cannot offer an effective constraint on it. Ω_m and w_0 can be tightly constrained by the VD observation, which is benefited from the large sample size. On the other hand, although the TD observation can measure absolute distances, its ability to constrain cosmological parameters is very limited (except for H_0) due to its small sample size.

In summary, the TD observation can only constrain H_0 strictly, but has weak ability to constrain other cosmological parameters. The VD observation is highly complementary with the TD observation, which could offer tight constraints on Ω_m and w_0. Therefore, we can see that the combination of VD and TD could significantly break the parameter degeneracy so that the constraint precisions meeting the standard of precision cosmology can be obtained. In the context of cosmological tensions between early and late universe, the observations of SGL provide an alternative way to precisely measure cosmological parameters in the late universe and explore the nature of dark energy.
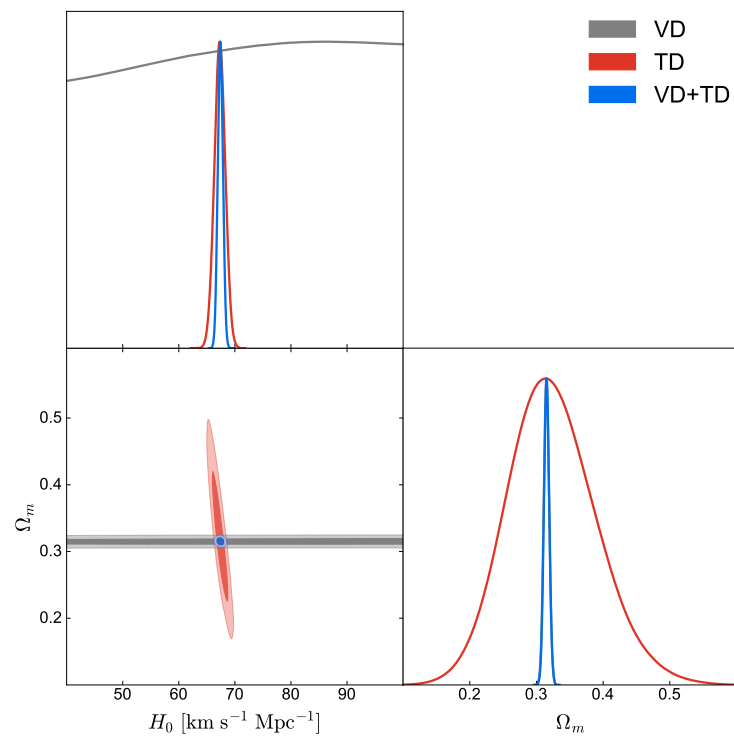
Figure 4. The constraints (68.3% and 95.4% confidence level) on the ΛCDM model from the simulations of VD, TD, and VD+TD.
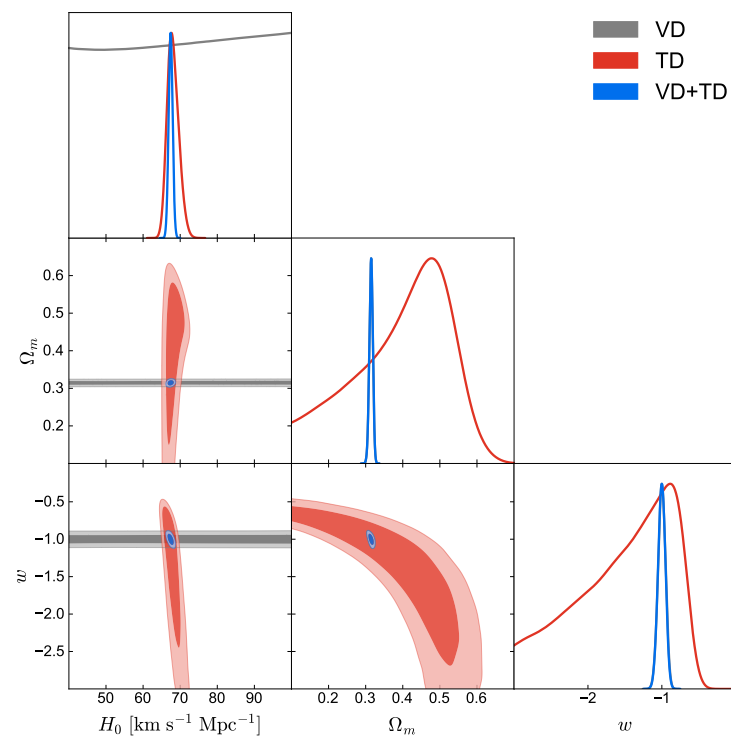
Figure 5. The constraints (68.3% and 95.4% confidence level) on the wCDM model from the simulations of VD, TD, and VD+TD.
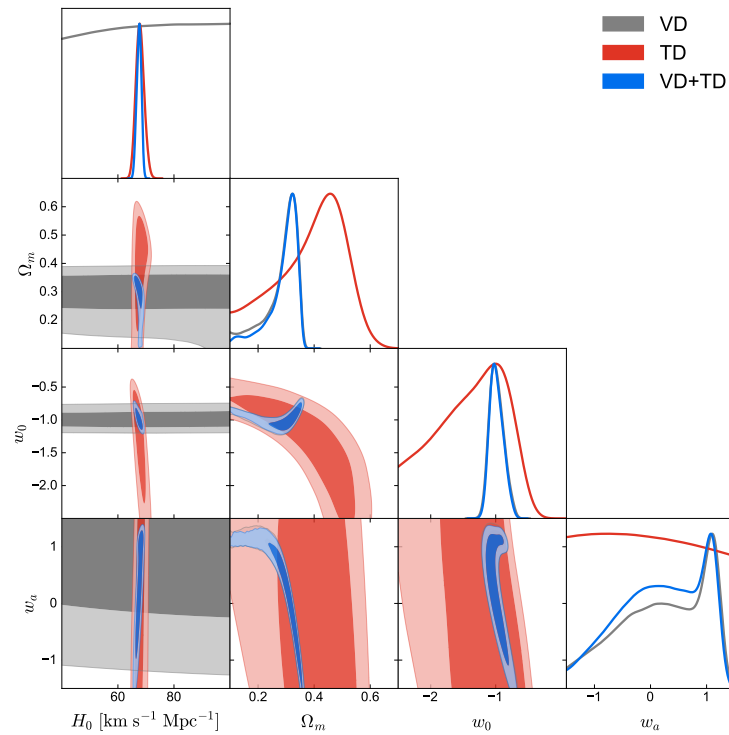
Figure 6. The constraints (68.3% and 95.4% confidence level) on the CPL model from the simulations of VD, TD, and VD+TD.

Table 3. The constraints on cosmological parameters of the ΛCDM, wCDM and CPL models by using the simulated VD, TD, and VD+TD. For comparison, we also list the fit results from the current CMB+BAO+SNe data, taken from Ref. [88]. Here, H_0 is in units of km s^{-1} Mpc^{-1}.

Model	Parameter	VD	TD	VD+TD	CMB+BAO+SNe
ΛCDM	H_0	-	$69.87^{+1.00}_{-1.02}$	69.99 ± 0.47	67.64 ± 0.44
	$\sigma(H_0)$	-	1.01	0.47	0.44
	Ω_{m}	0.300 ± 0.004	$0.310^{+0.068}_{-0.062}$	0.300 ± 0.004	0.314 ± 0.006
	$\sigma(\Omega_{\mathrm{m}})$	0.004	0.065	0.004	0.006
wCDM	H_0	-	$70.67^{+1.78}_{-1.52}$	$70.00^{+0.57}_{-0.56}$	67.90 ± 0.83
	$\sigma(H_0)$	-	1.65	0.57	0.83
	Ω_{m}	0.300 ± 0.005	$0.418^{+0.094}_{-0.160}$	$0.300^{+0.004}_{-0.005}$	0.312 ± 0.008
	$\sigma(\Omega_{\mathrm{m}})$	0.005	0.127	0.005	0.008
	w	-1.00 ± 0.05	$-1.44^{+0.56}_{-0.85}$	-1.00 ± 0.05	-1.01 ± 0.03
	$\sigma(w)$	0.05	0.71	0.05	0.03
CPL	H_0	-	$70.50^{+1.61}_{-1.48}$	$70.22^{+0.82}_{-0.96}$	67.91 ± 0.83
	$\sigma(H_0)$	-	1.55	0.89	0.83
	Ω_{m}	$0.289^{+0.032}_{-0.072}$	$0.403^{+0.095}_{-0.155}$	$0.288^{+0.031}_{-0.077}$	0.312 ± 0.008
	$\sigma(\Omega_{\mathrm{m}})$	0.052	0.125	0.054	0.008
	w_0	$-1.00^{+0.13}_{-0.10}$	$-1.36^{+0.49}_{-0.66}$	$-1.00^{+0.11}_{-0.09}$	-0.99 ± 0.08
	$\sigma(w_0)$	0.12	0.58	0.10	0.08
	w_a	$0.265^{+0.795}_{-0.910}$	$-0.069^{+1.053}_{-0.988}$	$0.288^{+0.769}_{-0.865}$	$-0.10^{+0.36}_{-0.27}$
	$\sigma(w_a)$	0.853	-	0.817	0.315

4. Conclusions

The increasingly improved measurements of cosmic distances including relative distances and absolute distances enable the remarkable development of cosmology and the precise constraints on some fundamental cosmological parameters. Meanwhile, however, the measured discrepancies among several key cosmological parameters have emerged

from the observations of early universe and late universe, which motivates us to explore the independent and precise late-universe probes. The two observed effects of SGL, time-delay measurements and the lens velocity dispersions, provide the measurements of absolute distances and relative distances, respectively, which are expected to break the cosmological parameter degeneracies and give tight constraints on them. In this paper, we combine the current observed 130 SGL systems with velocity dispersion and 7 SGL systems with time-delay measurements to constrain the ΛCDM, wCDM, and CPL models. We find that the TD observation is only sensitive to H_0 due to its absolute distance measurements. Moreover, the inference of H_0 from TD is strongly cosmological model dependent. In the ΛCDM model, the constraint on H_0 from the combination of VD and TD is $H_0 = 73.20^{+1.60}_{-1.86}$ km s^{-1} Mpc^{-1}, which is consistent with the results measured by local distance ladder from the SH0ES collaboration [89]. Compared with the constraints from individual VD and TD, the combination of them does not break significantly the degeneracy between cosmological parameters as expected.

It is worth noting that the choice of parametrization of total mass density slope γ has a significant influence on cosmological constraints [44,48,52]. In this paper, for the parametrization of γ, we take into account the dependencies of redshift and surface mass density, which introduces two additional lens model parameters, γ_z and γ_s. To eliminate the uncertainties of constrained cosmological parameters by introducing two additional lens model parameters, it is required to know how both the masses and sizes of galaxies change with time, which is poorly understood. Moreover, the influence of the prior of $\beta_{\rm ani}$ cannot be ignored [52], but its measurement is not very accurate at present. The lack of understanding of all these lens model parameters yields additional uncertainties in the estimation of cosmological parameters. As future massive surveys observe more and more SGL samples, a more accurate phenomenological model for lens galaxies could be characterized, which will greatly improve the constraint on cosmology using SGL data.

On the other hand, an abundant SGL sample with accurate measurements will be observed in the LSST era. We also make a forecast for the constraints on cosmological parameters from 8000 SGL systems with well-measured velocity dispersion and 55 SGL systems with well-measured time delay. We find that the TD observation with a small sample size can only constrain H_0 strictly, but has a very weak ability to constrain other cosmological parameters. The VD observation with a large sample size could be highly complementary with the TD observation to significantly break the parameter degeneracies. For example, for the wCDM model, the joint data analysis gives $\sigma(H_0) = 0.57$ km s^{-1} Mpc^{-1}, $\sigma(\Omega_m) = 0.005$ and $\sigma(w) = 0.05$, which are comparable with the results from Planck 2018 TT,TE,EE+lowE+lensing+SNe+BAO, and meet the standard of precision cosmology. We conclude that the observations of SGL will become a useful late-universe probe for precisely measuring cosmological parameters and exploring the nature of dark energy.

Author Contributions: Conceptualization, J.-Z.Q. and X.Z.; methodology, W.-H.H.; software, W.-H.H. and Y.C.; validation, W.-H.H.; formal analysis, J.-F.Z.; investigation, Y.C.; writing—original draft preparation, J.-Z.Q.; writing—review and editing, J.-F.Z.; supervision, J.-F.Z. and X.Z.; project administration, X.Z. All authors have read and agreed to the published version of the manuscript.

Institutional Review Board Statement: Not applicable.

Informed Consent Statement: Not applicable.

Data Availability Statement: Not applicable.

Conflicts of Interest: The authors declare no conflict of interest.

References

1. Bennett, C.L.; Halpern, M.; Hinshaw, G.; Jarosik, N.; Kogut, A.; Limon, M.; Meyer, S.S.; Page, L.; Spergel, D.N.; Tucker, G.S.; et al. First year Wilkinson Microwave Anisotropy Probe (WMAP) observations: Preliminary maps and basic results. *Astrophys. J. Suppl.* **2003**, *148*, 1–27. [CrossRef]
2. Spergel, D.N.; Verde, L.; Peiris, H.V.; Komatsu, E.; Nolta, M.R.; Bennett, C.L.; Halpern, M.; Hinshaw, G.; Jarosik, N.; Kogut, A.; et al. First year Wilkinson Microwave Anisotropy Probe (WMAP) observations: Determination of cosmological parameters. *Astrophys. J. Suppl.* **2003**, *148*, 175–194. [CrossRef]
3. Planck Collaboration; Aghanim, N.; Akrami, Y.; Ashdown, M.; Aumont, J.; Baccigalupi, C.; Ballardini, M.; Banday, A.J.; Barreiro, R.B.; Bartolo, N.; et al. Planck 2018 results. VI. Cosmological parameters. *Astron. Astrophys.* **2020**, *641*, A6. [CrossRef]
4. Riess, A.G.; Filippenko, A.V.; Challis, P.; Clocchiatti, A.; Diercks, A.; Garnavich, P.M.; Gillil, R.L.; Hogan, C.J.; Jha, S.; Kirshner, R.P.; et al. Observational evidence from supernovae for an accelerating universe and a cosmological constant. *Astron. J.* **1998**, *116*, 1009–1038. [CrossRef]
5. Perlmutter, S.; Aldering, G.; Goldhaber, G.; Knop, R.A.; Nugent, P.; Castro, P.G.; Deustua, S.; Fabbro, S.; Goobar, A.; Groom, D.E.; et al. Measurements of Ω and Λ from 42 high redshift supernovae. *Astrophys. J.* **1999**, *517*, 565–586. [CrossRef]
6. Eisenstein, D.J.; Zehavi, I.; Hogg, D.W.; Scoccimarro, R.; Blanton, M.R.; Nichol, R.C.; Scranton, R.; Seo, H.J.; Tegmark, M.; Zheng, Z.; et al. Detection of the Baryon Acoustic Peak in the Large-Scale Correlation Function of SDSS Luminous Red Galaxies. *Astrophys. J.* **2005**, *633*, 560–574. [CrossRef]
7. Alam, S.; Ata, M.; Bailey, S.; Beutler, F.; Bizyaev, D.; Blazek, J.A.; Bolton, A.S.; Brownstein, J.R.; Burden, A.; Chuang, C.H.; et al. The clustering of galaxies in the completed SDSS-III Baryon Oscillation Spectroscopic Survey: Cosmological analysis of the DR12 galaxy sample. *Mon. Not. R. Astron. Soc.* **2017**, *470*, 2617–2652. [CrossRef]
8. Di Valentino, E.; Mena, O.; Pan, S.; Visinelli, L.; Yang, W.; Melchiorri, A.; Mota, D.F.; Riess, A.G.; Silk, J. In the realm of the Hubble tension—A review of solutions. *Class. Quant. Grav.* **2021**, *38*, 153001. [CrossRef]
9. Vagnozzi, S. New physics in light of the H_0 tension: An alternative view. *Phys. Rev. D* **2020**, *102*, 023518. [CrossRef]
10. Zhang, X. Gravitational wave standard sirens and cosmological parameter measurement. *Sci. China Phys. Mech. Astron.* **2019**, *62*, 110431. [CrossRef]
11. Qi, J.Z.; Zhang, X. A new cosmological probe using super-massive black hole shadows. *Chin. Phys. C* **2020**, *44*, 055101. [CrossRef]
12. Guo, R.Y.; Zhang, L.; Zhang, J.F.; Zhang, X. Constraints on brane inflation after Planck 2015: Impacts of the latest local measurement of the Hubble constant. *Sci. China Phys. Mech. Astron.* **2019**, *62*, 30411. [CrossRef]
13. Vattis, K.; Koushiappas, S.M.; Loeb, A. Dark matter decaying in the late Universe can relieve the H0 tension. *Phys. Rev. D* **2019**, *99*, 121302. [CrossRef]
14. Guo, R.Y.; Zhang, J.F.; Zhang, X. Inflation model selection revisited after a 1.91% measurement of the Hubble constant. *Sci. China Phys. Mech. Astron.* **2020**, *63*, 290406. [CrossRef]
15. Zhang, J.F.; Geng, J.J.; Zhang, X. Neutrinos and dark energy after Planck and BICEP2: Data consistency tests and cosmological parameter constraints. *JCAP* **2014**, *10*, 044. [CrossRef]
16. Guo, R.Y.; Zhang, J.F.; Zhang, X. Can the H_0 tension be resolved in extensions to ΛCDM cosmology? *JCAP* **2019**, *02*, 054. [CrossRef]
17. Zhao, M.M.; He, D.Z.; Zhang, J.F.; Zhang, X. Search for sterile neutrinos in holographic dark energy cosmology: Reconciling Planck observation with the local measurement of the Hubble constant. *Phys. Rev. D* **2017**, *96*, 043520. [CrossRef]
18. Guo, R.Y.; Zhang, X. Constraints on inflation revisited: An analysis including the latest local measurement of the Hubble constant. *Eur. Phys. J. C* **2017**, *77*, 882. [CrossRef]
19. Feng, L.; He, D.Z.; Li, H.L.; Zhang, J.F.; Zhang, X. Constraints on active and sterile neutrinos in an interacting dark energy cosmology. *Sci. China Phys. Mech. Astron.* **2020**, *63*, 290404. [CrossRef]
20. Liu, M.; Huang, Z.; Luo, X.; Miao, H.; Singh, N.K.; Huang, L. Can Non-Standard Recombination Resolve the Hubble Tension? *Sci. China Phys. Mech. Astron.* **2020**, *63*, 290405. [CrossRef]
21. Zhang, X.; Huang, Q.G. Measuring H0 from low-z datasets. *Sci. China Phys. Mech. Astron.* **2020**, *63*, 290402. [CrossRef]
22. Ding, Q.; Nakama, T.; Wang, Y. A gigaparsec-scale local void and the Hubble tension. *Sci. China Phys. Mech. Astron.* **2020**, *63*, 290403. [CrossRef]
23. Riess, A.G.; Casertano, S.; Yuan, W.; Macri, L.M.; Scolnic, D. Large Magellanic Cloud Cepheid Standards Provide a 1% Foundation for the Determination of the Hubble Constant and Stronger Evidence for Physics beyond ΛCDM. *Astrophys. J.* **2019**, *876*, 85. [CrossRef]

24. Di Valentino, E.; Melchiorri, A.; Fantaye, Y.; Heavens, A. Bayesian evidence against the Harrison-Zel'dovich spectrum in tensions with cosmological data sets. *Phys. Rev. D* **2018**, *98*, 063508. [CrossRef]

25. Wong, K.C.; Suyu, S.H.; Chen, G.C.; Rusu, C.E.; Millon, M.; Sluse, D.; Bonvin, V.; Fassnacht, C.D.; Taubenberger, S.; Auger, M.W.; et al. H0LiCOW–XIII. A 2.4 per cent measurement of H0 from lensed quasars: 5.3σ tension between early- and late-Universe probes. *Mon. Not. R. Astron. Soc.* **2020**, *498*, 1420–1439. [CrossRef]

26. Millon, M.; Galan, A.; Courbin, F.; Treu, T.; Suyu, S.H.; Ding, X.; Birrer, S.; Chen, G.F.; Shajib, A.J.; Sluse, D.; et al. TDCOSMO. I. An exploration of systematic uncertainties in the inference of H_0 from time-delay cosmography. *Astron. Astrophys.* **2020**, *639*, A101. [CrossRef]

27. Rusu, C.E.; Wong, K.C.; Bonvin, V.; Sluse, D.; Suyu, S.H.; Fassnacht, C.D.; Chan, J.H.; Hilbert, S.; Auger, M.W.; Sonnenfeld, A.; et al. H0LiCOW XII. Lens mass model of WFI2033-4723 and blind measurement of its time-delay distance and H0. *Mon. Not. R. Astron. Soc.* **2020**, *498*, 1440–1468. [CrossRef]

28. Chen, G.C.; Fassnacht, C.D.; Suyu, S.H.; Rusu, C.E.; Chan, J.H.; Wong, K.C.; Auger, M.W.; Hilbert, S.; Bonvin, V.; Birrer, S.; et al. A SHARP view of H0LiCOW: H_0 from three time-delay gravitational lens systems with adaptive optics imaging. *Mon. Not. R. Astron. Soc.* **2019**, *490*, 1743–1773. [CrossRef]

29. Shajib, A.J.; Birrer, S.; Treu, T.; Agnello, A.; Buckley-Geer, E.J.; Chan, J.H.H.; Christensen, L.; Lemon, C.; Lin, H.; Millon, M.; et al. STRIDES: A 3.9 per cent measurement of the Hubble constant from the strong lens system DES J0408-5354. *Mon. Not. R. Astron. Soc.* **2020**, *494*, 6072–6102. [CrossRef]

30. Ivezić, Ž; Kahn, S.M.; Tyson, J.A.; Abel, B.; Acosta, E.; Allsman, R.; Alonso, D.; AlSayyad, Y.; Anderson, S.F.; Andrew, J.; et al. LSST: From Science Drivers to Reference Design and Anticipated Data Products. *Astrophys. J.* **2019**, *873*, 111. [CrossRef]

31. Huber, S.; Suyu, S.H.; Noebauer, U.M.; Bonvin, V.; Rothchild, D.; Chan, J.H.H.; Awan, H.; Courbin, F.; Kromer, M.; Marshall, P.; et al. Strongly lensed SNe Ia in the era of LSST: Observing cadence for lens discoveries and time-delay measurements. *Astron. Astrophys.* **2019**, *631*, A161. [CrossRef]

32. Jee, I.; Komatsu, E.; Suyu, S.H.; Huterer, D. Time-delay Cosmography: Increased Leverage with Angular Diameter Distances. *JCAP* **2016**, *04*, 031. [CrossRef]

33. Wen, X.; Liao, K. Calibrating the standard candles with strong lensing. *Eur. Phys. J. C* **2020**, *80*, 94. [CrossRef]

34. Shajib, A.J.; Treu, T.; Agnello, A. Improving time-delay cosmography with spatially resolved kinematics. *Mon. Not. R. Astron. Soc.* **2018**, *473*, 210–226. [CrossRef]

35. Dev, A.; Jain, D.; Mahajan, S. Dark energy and the statistical study of the observed image separations of the multiply imaged systems in the class statistical sample. *Int. J. Mod. Phys. D* **2004**, *13*, 1005–1018. [CrossRef]

36. Cao, S.; Covone, G.; Zhu, Z.H. Testing the dark energy with gravitational lensing statistics. *Astrophys. J.* **2012**, *755*, 31. [CrossRef]

37. Mitchell, J.L.; Keeton, C.R.; Frieman, J.A.; Sheth, R.K. Robust cosmological constraints from gravitational lens statistics. *Astrophys. J.* **2005**, *622*, 81–98. [CrossRef]

38. Cao, S.; Zhu, Z.H. Constraints on cosmological models from lens redshift data. *Astron. Astrophys.* **2012**, *538*, A43. [CrossRef]

39. Ma, Y.B.; Cao, S.; Zhang, J.; Geng, S.; Liu, Y.; Liu, T.; Pan, Y. Implications of the lens redshift distribution of strong lensing systems: Cosmological parameters and the global properties of early-type galaxies. *Eur. Phys. J. C* **2019**, *79*, 121. [CrossRef]

40. Biesiada, M. Strong lensing systems as a probe of dark energy in the universe. *Phys. Rev. D* **2006**, *73*, 023006. [CrossRef]

41. Grillo, C.; Lombardi, M.; Bertin, G. Cosmological parameters from strong gravitational lensing and stellar dynamics in elliptical galaxies. *Astron. Astrophys.* **2008**, *477*, 397. [CrossRef]

42. Schwab, J.; Bolton, A.S.; Rappaport, S.A. Galaxy-Scale Strong Lensing Tests of Gravity and Geometric Cosmology: Constraints and Systematic Limitations. *Astrophys. J.* **2010**, *708*, 750–757. [CrossRef]

43. Cao, S.; Biesiada, M.; Gavazzi, R.; Piórkowska, A.; Zhu, Z.H. Cosmology With Strong-lensing Systems. *Astrophys. J.* **2015**, *806*, 185. [CrossRef]

44. Qi, J.Z.; Cao, S.; Zhang, S.; Biesiada, M.; Wu, Y.; Zhu, Z.H. The distance sum rule from strong lensing systems and quasars—Test of cosmic curvature and beyond. *Mon. Not. R. Astron. Soc.* **2019**, *483*, 1104–1113. [CrossRef]

45. Li, Z.; Ding, X.; Wang, G.J.; Liao, K.; Zhu, Z.H. Curvature from strong gravitational lensing: A spatially closed Universe or systematics? *Astrophys. J.* **2018**, *854*, 146. [CrossRef]

46. Cui, J.L.; Li, H.L.; Zhang, X. No evidence for the evolution of mass density power-law index γ from strong gravitational lensing observation. *Sci. China Phys. Mech. Astron.* **2017**, *60*, 080411. [CrossRef]

47. Cao, S.; Li, X.; Biesiada, M.; Xu, T.; Cai, Y.; Zhu, Z.H. Test of parametrized post-Newtonian gravity with galaxy-scale strong lensing systems. *Astrophys. J.* **2017**, *835*, 92. [CrossRef]

48. Wang, B.; Qi, J.Z.; Zhang, J.F.; Zhang, X. Cosmological Model-independent Constraints on Spatial Curvature from Strong Gravitational Lensing and SN Ia Observations. *Astrophys. J.* **2020**, *898*, 100. [CrossRef]

49. Wang, Y.J.; Qi, J.Z.; Wang, B.; Zhang, J.F.; Cui, J.L.; Zhang, X. Cosmological model-independent measurement on cosmic curvature using distance sum rule with the help of gravitational waves. *arXiv* **2022**, arXiv:2201.12553.

50. Wei, J.J.; Chen, Y.; Cao, S.; Wu, X.F. Direct Estimate of the Post-Newtonian Parameter and Cosmic Curvature from Galaxy-scale Strong Gravitational Lensing. *Astrophys. J. Lett.* **2022**, *927*, L1. [CrossRef]

51. Geng, S.; Cao, S.; Liu, Y.; Liu, T.; Biesiada, M.; Lian, Y. The velocity dispersion function of early-type galaxies and its redshift evolution: The newest results from lens redshift test. *Mon. Not. R. Astron. Soc.* **2021**, *503*, 1319–1326. [CrossRef]

52. Chen, Y.; Li, R.; Shu, Y.; Cao, X. Assessing the effect of lens mass model in cosmological application with updated galaxy-scale strong gravitational lensing sample. *Mon. Not. R. Astron. Soc.* **2019**, *488*, 3745–3758. [CrossRef]
53. Liu, X.H.; Li, Z.H.; Qi, J.Z.; Zhang, X. Galaxy-Scale Test of General Relativity with Strong Gravitational Lensing. *Astrophys. J.* **2022**, *927*, 28. [CrossRef]
54. Qi, J.Z.; Cui, Y.; Hu, W.H.; Zhang, J.F.; Cui, J.L.; Zhang, X. Strongly lensed type Ia supernovae as a precise late-universe probe of measuring the Hubble constant and cosmic curvature. *arXiv* **2022**, arXiv:2202.01396.
55. Oguri, M.; Marshall, P.J. Gravitationally lensed quasars and supernovae in future wide-field optical imaging surveys. *Mon. Not. R. Astron. Soc.* **2010**, *405*, 2579–2593. [CrossRef]
56. Collett, T.E. The population of galaxy-galaxy strong lenses in forthcoming optical imaging surveys. *Astrophys. J.* **2015**, *811*, 20. [CrossRef]
57. Goldstein, D.A.; Nugent, P.E.; Goobar, A. Rates and Properties of Supernovae Strongly Gravitationally Lensed by Elliptical Galaxies in Time-domain Imaging Surveys. *Astrophys. J. Suppl.* **2019**, *243*, 6. [CrossRef]
58. Wojtak, R.; Hjorth, J.; Gall, C. Magnified or multiply imaged? – Search strategies for gravitationally lensed supernovae in wide-field surveys. *Mon. Not. R. Astron. Soc.* **2019**, *487*, 3342–3355. [CrossRef]
59. Cao, S.; Pan, Y.; Biesiada, M.; Godlowski, W.; Zhu, Z.H. Constraints on cosmological models from strong gravitational lensing systems. *JCAP* **2012**, *03*, 016. [CrossRef]
60. Cao, S.; Zhu, Z.H. Cosmic equation of state from combined angular diameter distances: Does the tension with luminosity distances exist? *Phys. Rev. D* **2014**, *90*, 083006. [CrossRef]
61. Li, X.L.; Cao, S.; Zheng, X.G.; Li, S.; Biesiada, M. Comparison of cosmological models using standard rulers and candles. *Res. Astron. Astrophys.* **2016**, *16*, 084. [CrossRef]
62. Qi, J.Z.; Zhao, J.W.; Cao, S.; Biesiada, M.; Liu, Y. Measurements of the Hubble constant and cosmic curvature with quasars: Ultracompact radio structure and strong gravitational lensing. *Mon. Not. R. Astron. Soc.* **2021**, *503*, 2179–2186. [CrossRef]
63. Cao, M.D.; Zheng, J.; Qi, J.Z.; Zhang, X.; Zhu, Z.H. A new way to explore cosmological tensions using gravitational waves and strong gravitational lensing. *arXiv* **2021**, arXiv:2112.14564
64. Wu, P.J.; Shao, Y.; Jin, S.J.; Zhang, X. A path to precision cosmology: Synergy between four promising late-universe cosmological probes. *arXiv* **2022**, arXiv:2202.09726.
65. Suyu, S.H.; Treu, T.; Hilbert, S.; Sonnenfeld, A.; Auger, M.W.; Blandford, R.D.; Collett, T.; Courbin, F.; Fassnacht, C.D.; Koopmans, L.V.; et al. Cosmology from gravitational lens time delays and Planck data. *Astrophys. J. Lett.* **2014**, *788*, L35. [CrossRef]
66. Verde, L.; Treu, T.; Riess, A.G. Tensions between the Early and the Late Universe. *Nat. Astron.* **2019**, *3*, 891. [CrossRef]
67. Linder, E.V. Exploring the expansion history of the universe. *Phys. Rev. Lett.* **2003**, *90*, 091301. [CrossRef]
68. Kormann, R.; Schneider, P.; Bartelmann, M. Isothermal elliptical gravitational lens models. *Astron. Astrophys.* **1994**, *284*, 285–299.
69. Asada, H.; Hamana, T.; Kasai, M. Images for an isothermal ellipsoidal gravitational lens from a single real algebraic equation. *Astron. Astrophys.* **2003**, *397*, 825. [CrossRef]
70. Koopmans, L.V.E. Gravitational lensing & stellar dynamics. *EAS Publ. Ser.* **2006**, *20*, 161. [CrossRef]
71. Jorgensen, I.; Franx, M.; Kjaergaard, P. Spectroscopy for E and S0 galaxies in nine clusters. *Mon. Not. R. Astron. Soc.* **1995**, *276*, 1341–1364.
72. Jiang, G.; Kochanek, C.S. The Baryon Fractions and Mass-to-Light Ratios of Early-Type Galaxies. *Astrophys. J.* **2007**, *671*, 1568. [CrossRef]
73. Schechter, P.L.; Bailyn, C.D.; Barr, R.; Barvainis, R.; Becker, C.M.; Bernstein, G.M.; Blakeslee, J.P.; Bus, S.J.; Dressler, A.; Falco, E.E.; et al. The Quadruple gravitational lens PG1115+080: Time delays and models. *Astrophys. J. Lett.* **1997**, *475*, L85–L88. [CrossRef]
74. Fassnacht, C.D.; Pearson, T.J.; Readhead, A.C.S.; Browne, I.W.A.; Koopmans, L.V.E.; Myers, S.T.; Wilkinson, P.N. A determination of h_0 with the class gravitational lens b1608+656: I. time delay measurements with the vla. *Astrophys. J.* **1999**, *527*, 498. [CrossRef]
75. Fassnacht, C.D.; Xanthopoulos, E.; Koopmans, L.V.E.; Rusin, D. A determination of H(O) with the class gravitational lens B1608+656. 3. A Significant improvement in the precision of the time delay measurements. *Astrophys. J.* **2002**, *581*, 823–835. [CrossRef]
76. Kochanek, C.S.; Morgan, N.D.; Falco, E.E.; McLeod, B.A.; Winn, J.N.; Dembicky, J.; Ketzeback, B. The Time delays of gravitational lens HE0435-1223: An Early-type galaxy with a rising rotation curve. *Astrophys. J.* **2006**, *640*, 47–61. [CrossRef]
77. Courbin, F.; Chantry, V.; Revaz, Y.; Sluse, D.; Faure, C.; Tewes, M.; Eulaers, E.; Koleva, M.; Asfandiyarov, I.; Dye, S.; et al. COSMOGRAIL: The COSmological MOnitoring of GRAvItational Lenses IX. Time delays, lens dynamics and baryonic fraction in HE 0435-1223. *Astron. Astrophys.* **2011**, *536*, A53. [CrossRef]
78. Refsdal, S. On the possibility of determining Hubble's parameter and the masses of galaxies from the gravitational lens effect. *Mon. Not. R. Astron. Soc.* **1964**, *128*, 307. [CrossRef]
79. Suyu, S.H.; Marshall, P.J.; Auger, M.W.; Hilbert, S.; Blandford, R.D.; Koopmans, L.V.E.; Fassnacht, C.D.; Treu, T. Dissecting the Gravitational Lens B1608+656. II. Precision Measurements of the Hubble Constant, Spatial Curvature, and the Dark Energy Equation of State. *Astrophys. J.* **2010**, *711*, 201–221. [CrossRef]
80. Bonvin, V.; Courbin, F.; Suyu, S.H.; Marshall, P.J.; Rusu, C.E.; Sluse, D.; Tewes, M.; Wong, K.C.; Collett, T.; Fassnacht, C.D.; et al. H0LiCOW–V. New COSMOGRAIL time delays of HE 0435-1223: H_0 to 3.8 per cent precision from strong lensing in a flat ΛCDM model. *Mon. Not. R. Astron. Soc.* **2017**, *465*, 4914–4930. [CrossRef]

81. Jee, I.; Suyu, S.; Komatsu, E.; Fassnacht, C.D.; Hilbert, S.; Koopmans, L.V.E. A measurement of the Hubble constant from angular diameter distances to two gravitational lenses. *Science* **2019**, *365*, 1134–1138. [CrossRef] [PubMed]

82. Wong, K.C.; Suyu, S.H.; Auger, M.W.; Bonvin, V.; Courbin, F.; Fassnacht, C.D.; Halkola, A.; Rusu, C.E.; Sluse, D.; Sonnenfeld, A.; et al. H0LiCOW–IV. Lens mass model of HE 0435-1223 and blind measurement of its time-delay distance for cosmology. *Mon. Not. R. Astron. Soc.* **2017**, *465*, 4895–4913. [CrossRef]

83. Birrer, S.; Treu, T.; Rusu, C.E.; Bonvin, V.; Fassnacht, C.D.; Chan, J.H.H.; Agnello, A.; Shajib, A.J.; Chen, G.C.; Auger, M.; et al. H0LiCOW–IX. Cosmographic analysis of the doubly imaged quasar SDSS 1206+4332 and a new measurement of the Hubble constant. *Mon. Not. R. Astron. Soc.* **2019**, *484*, 4726. [CrossRef]

84. Agnello, A.; Lin, H.; Buckley-Geer, L.; Treu, T.; Bonvin, V.; Courbin, F.; Lemon, C.; Morishita, T.; Amara, A.; Auger, M.W.; et al. Models of the strongly lensed quasar DES J0408-5354. *Mon. Not. R. Astron. Soc.* **2017**, *472*, 4038–4050. [CrossRef]

85. Foreman-Mackey, D.; Hogg, D.W.; Lang, D.; Goodman, J. emcee: The MCMC Hammer. *Publ. Astron. Soc. Pac.* **2013**, *125*, 306–312. [CrossRef]

86. Suyu, S.H.; Bonvin, V.; Courbin, F.; Fassnacht, C.D.; Rusu, C.E.; Sluse, D.; Treu, T.; Wong, K.C.; Auger, M.W.; Ding, X.; et al. H0LiCOW–I. H0 Lenses in COSMOGRAIL's Wellspring: Program overview. *Mon. Not. R. Astron. Soc.* **2017**, *468*, 2590–2604. [CrossRef]

87. Suyu, S.H.; Huber, S.; Cañameras, R.; Kromer, M.; Schuldt, S.; Taubenberger, S.; Yıldırım, A.; Bonvin, V.; Chan, J.H.H.; Courbin, F.; et al. HOLISMOKES–I. Highly Optimised Lensing Investigations of Supernovae, Microlensing Objects, and Kinematics of Ellipticals and Spirals. *Astron. Astrophys.* **2020**, *644*, A162. [CrossRef]

88. Zhang, J.F.; Zhang, M.; Jin, S.J.; Qi, J.Z.; Zhang, X. Cosmological parameter estimation with future gravitational wave standard siren observation from the Einstein Telescope. *JCAP* **2019**, *09*, 068. [CrossRef]

89. Riess, A.G.; Casertano, S.; Yuan, W.; Bowers, J.B.; Macri, L.; Zinn, J.C.; Scolnic, D. Cosmic Distances Calibrated to 1% Precision with Gaia EDR3 Parallaxes and Hubble Space Telescope Photometry of 75 Milky Way Cepheids Confirm Tension with ΛCDM. *Astrophys. J. Lett.* **2021**, *908*, L6. [CrossRef]